High-Precision Detection of Ordinary Sound by Electrospun Polyacrylonitrile Nanofibers

Lu Peng,[1,a] Xin Jin,[1,b] Jiarong Niu,[a] Wenyu Wang,[*a] Hongxia Wang,[c] Hao Shao,[c] Chenhong Lang [d] and Tong Lin [*c]

[a] *State Key Laboratory of Separation Membranes and Membrane Processes, School of Textile Science and Engineering, Tiangong University, Tianjin 300387, P. R. China*

[b] *State Key Laboratory of Separation Membranes and Membrane Processes, School of Materials Science and Engineering, Tiangong University, Tianjin 300387, P. R. China*

[c] *Institute for Frontier Materials, Deakin University, Geelong, Victoria 3216, Australia*

[d] *College of Textiles and Apparel, Quanzhou Normal University, Quanzhou, 362000, China*

1 Both authors contributed equally to the manuscript.

Corresponding authors' emails: wwy-322@126.com
tong.lin@deakin.edu.au

Electronic Supplementary Information

Calculation of zigzag conformation content

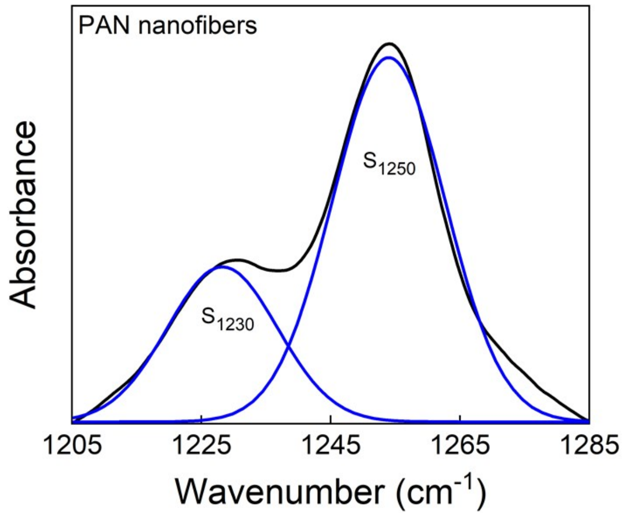

Fig. S1. FTIR spectra of the PAN nanofiber membrane in the wavenumber range of 1205 cm^{-1} to 1285 cm^{-1}.

The vibration bands at 1250 cm^{-1} and 1230 cm^{-1} were corresponded to zigzag conformation and 3^1-helical conformation, respectively. Based on the FTIR spectra, the zigzag conformation content (Φ) was estimated using the equation (S-1):

$$\Phi=S_{1250}/(S_{1250}+S_{1230}) \qquad \text{(S-1)}$$

where S_{1250} and S_{1230} are the peaks at 1250 cm^{-1} and 1230 cm^{-1}, respectively.

Calculation of β phase content

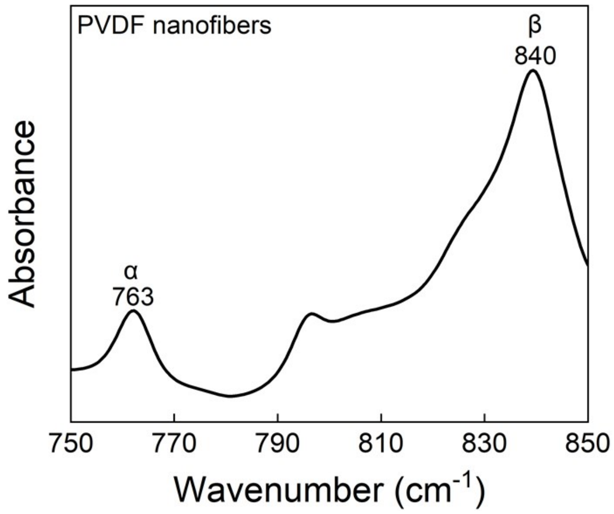

Fig. S2. FTIR spectra of the PVDF nanofiber membrane in the wavenumber range of 750 cm^{-1} to 850 cm^{-1}.

The FTIR spectrum showed characteristic vibration bands assigned to the PVDF β phases at 840 cm^{-1} (CH_2 rocking and CF_2 asymmetrical stretching vibration) and 1276 cm^{-1} (C-F stretching vibration). The characteristic bands associated with the α crystal phase were found at 613 cm^{-1} (CF_2 bending and CCC skeletal vibration), 763 cm^{-1} (CH_2 in-plane or rocking), and 975 cm^{-1} (CH_2 twisting). Based on the FTIR result, the β phases content of PVDF can be calculated using the equation (S-2):

$$F(\beta)=A_{\beta}/(1.26\ A_{\alpha}+A_{\beta}) \qquad \text{(S-2)}$$

A_{α} and A_{β} are the intensity of the β phase peak at 840 cm^{-1} and the intensity of the α crystal phase peak at 763 cm^{-1}, respectively.

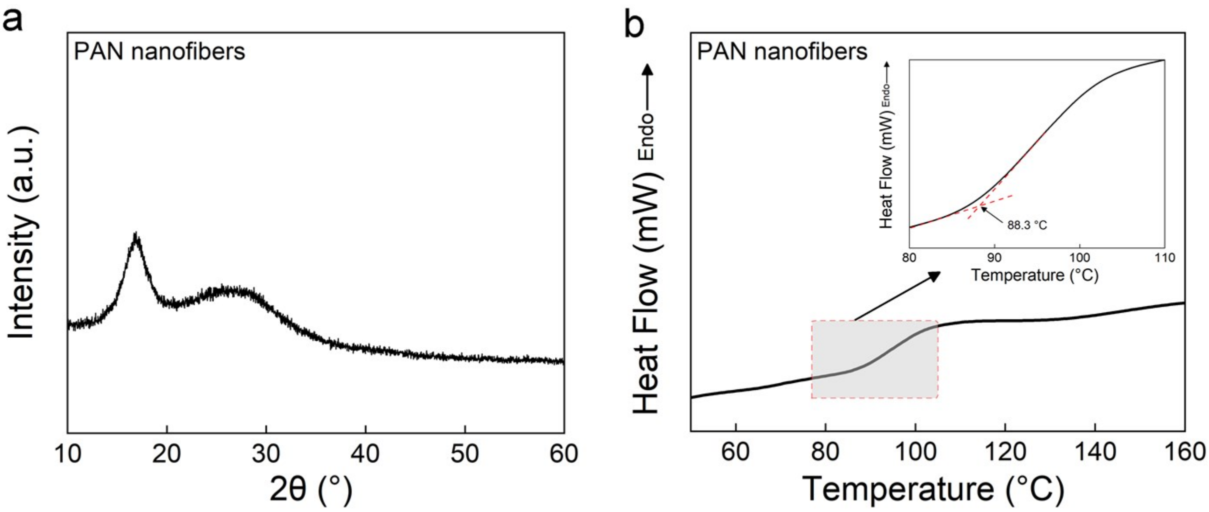

Fig. S3. (a) XRD pattern and (b) DSC curves of the PAN nanofiber membrane.

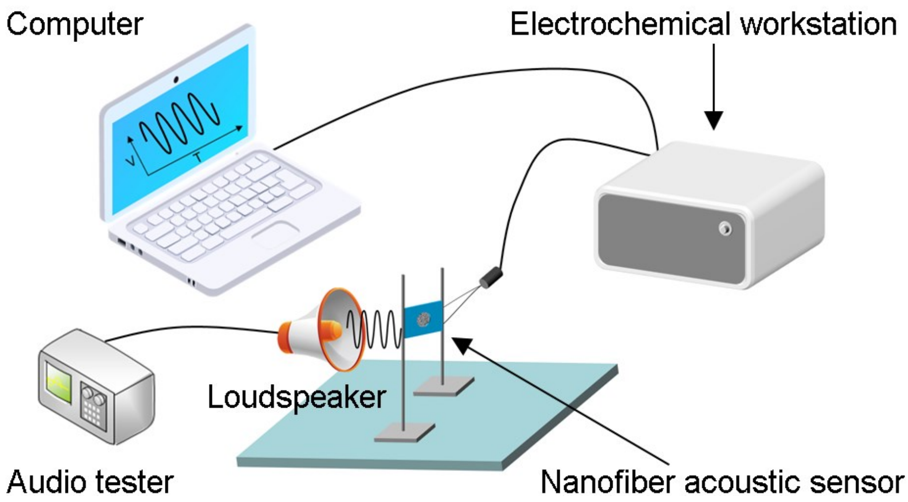

Fig. S4. Schematic illustration of the setup for testing the nanofiber devices.

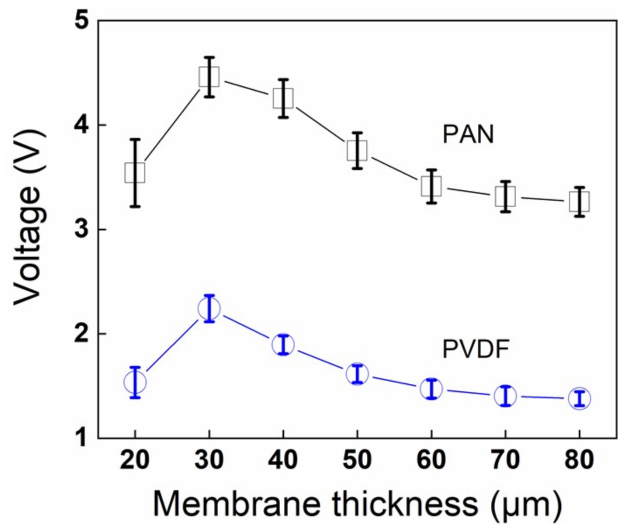

Fig. S5. Effect of nanofiber membrane thickness on energy conversion performance under 200 Hz 115dB sound. The error bars represent the standard deviation obtained from the test results of at least three replicates.

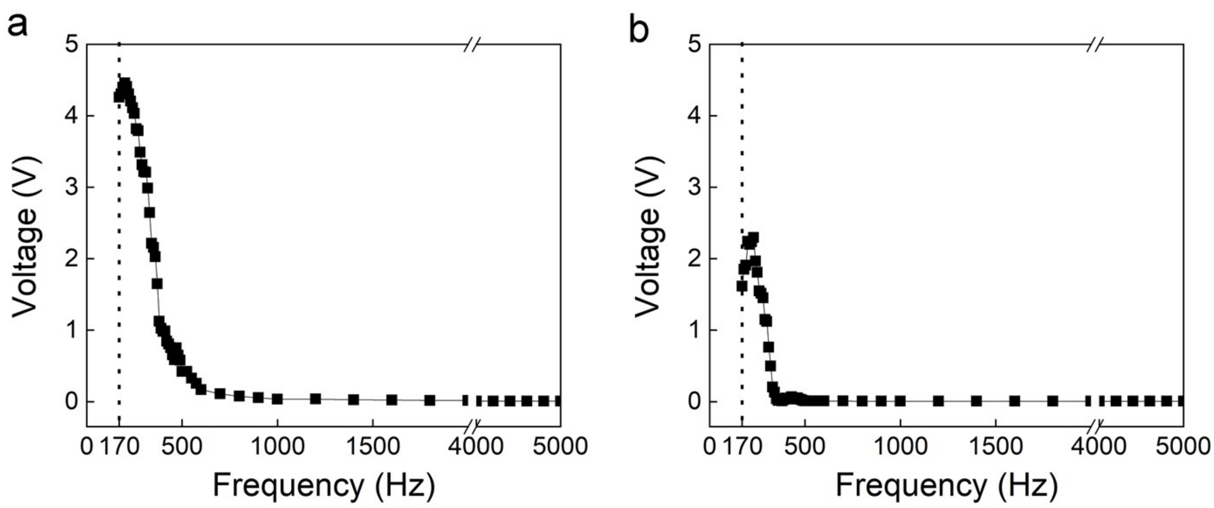

Fig. S6. Effect of sound frequency on voltage signal outputs for (a) PAN and (b) PVDF under 115 dB sound. (Nanofiber membrane thickness, 30 μm)

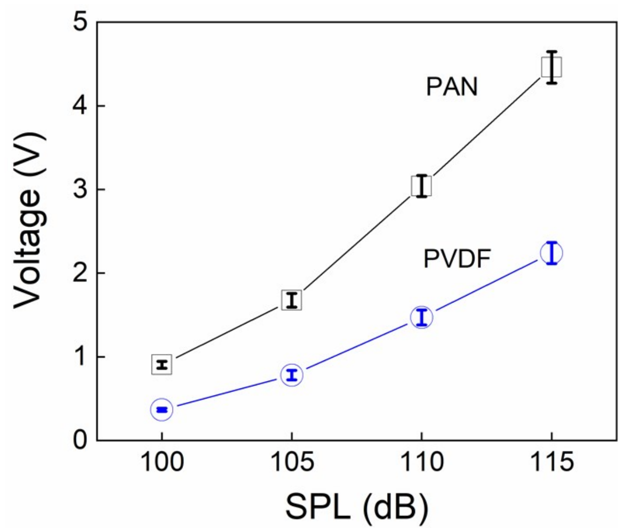

Fig. S7. Effect of SPL on voltage signal outputs for the PAN and PVDF membranes under 200 Hz sound. (Nanofiber membrane thickness, 30 μm)

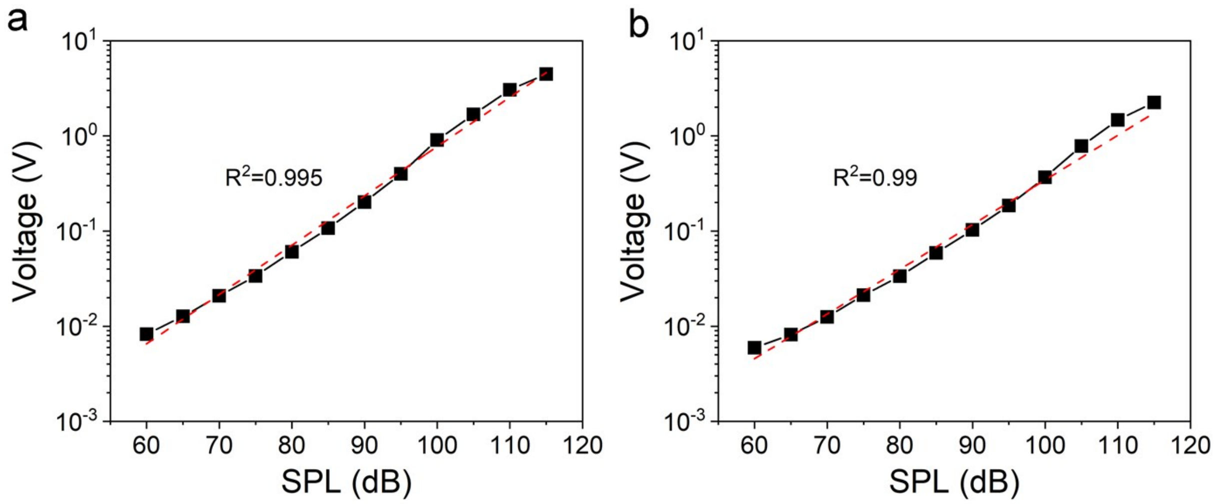

Fig. S8. The linear dependency of voltage output (logarithmic coordinate) on SPL. (Nanofiber membrane thickness, 30 μm)

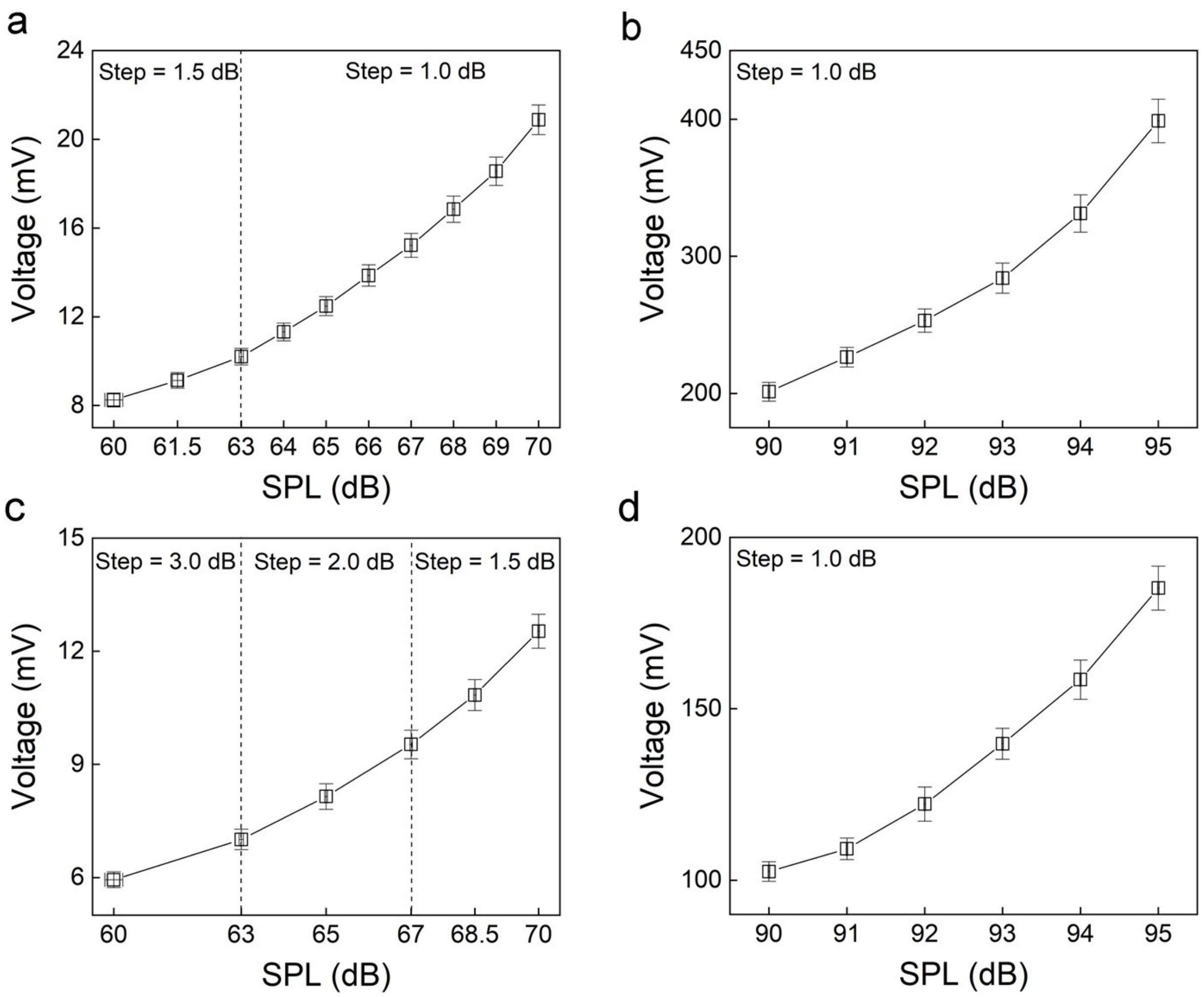

Fig. S9. The accuracy analysis of the PAN sensor device in (a) 60-70 dB and (b) 90-95 dB. The accuracy analysis of the PVDF device (c) 60-70 dB and (d) 90-95 dB. (sound frequency 200Hz)

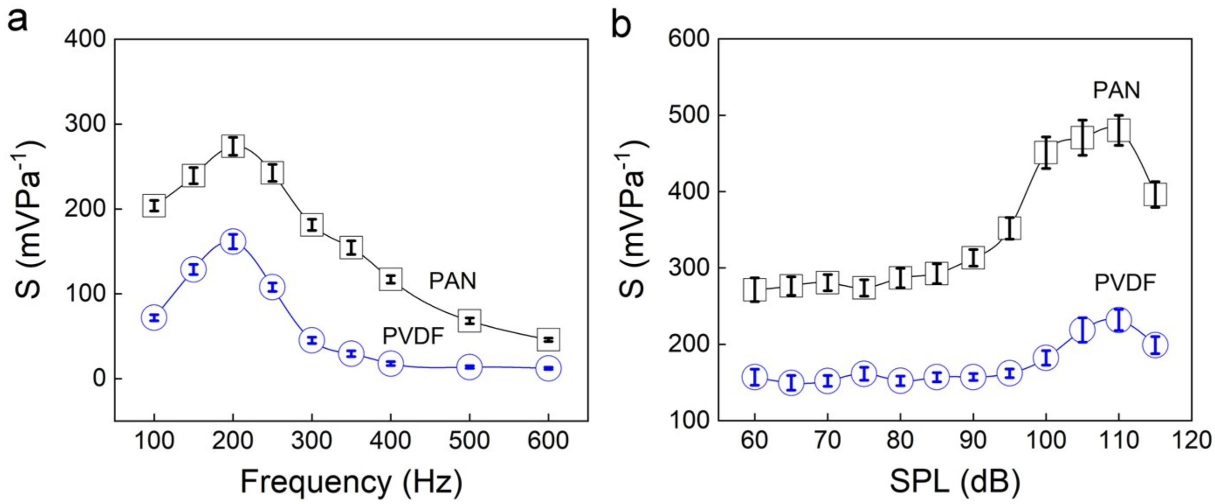

Fig. S10. The sensitivity of the PAN and PVDF nanofiber sensors at different (a) sound frequency (SPL, 75dB), and (b) SPL (sound frequency, 200Hz). (Membrane thickness, 30 μm)

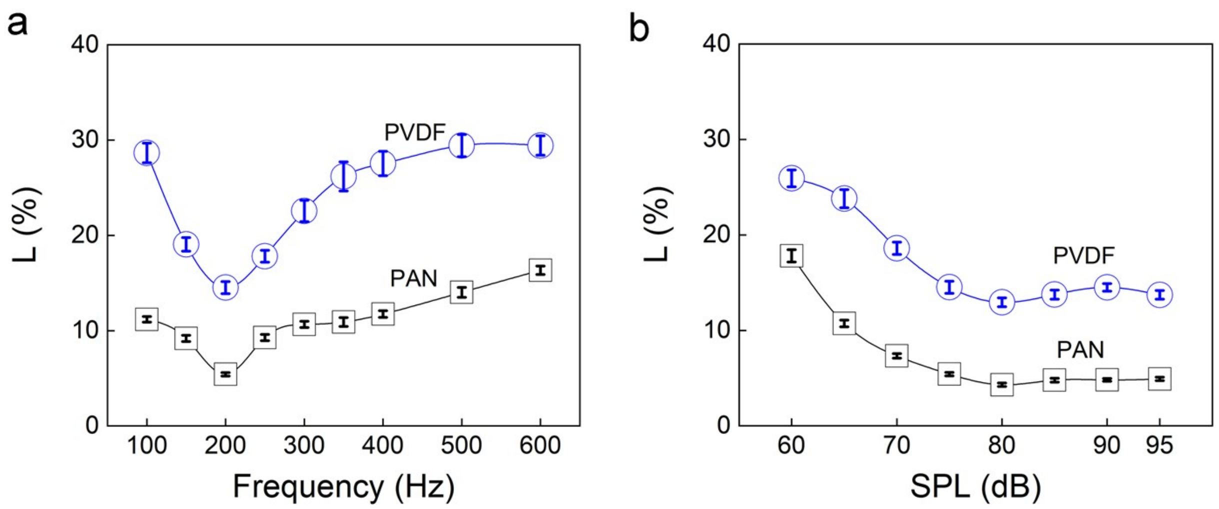

Fig. S11. *L* value of the PAN and PVDF nanofiber sensors for the conversion of the sinusoidal sound wave at different conditions. (a) different sound frequencies (SPL, 75dB), and (b) different SPLs (sound frequency, 200Hz). (Membrane thickness, 30 μm)

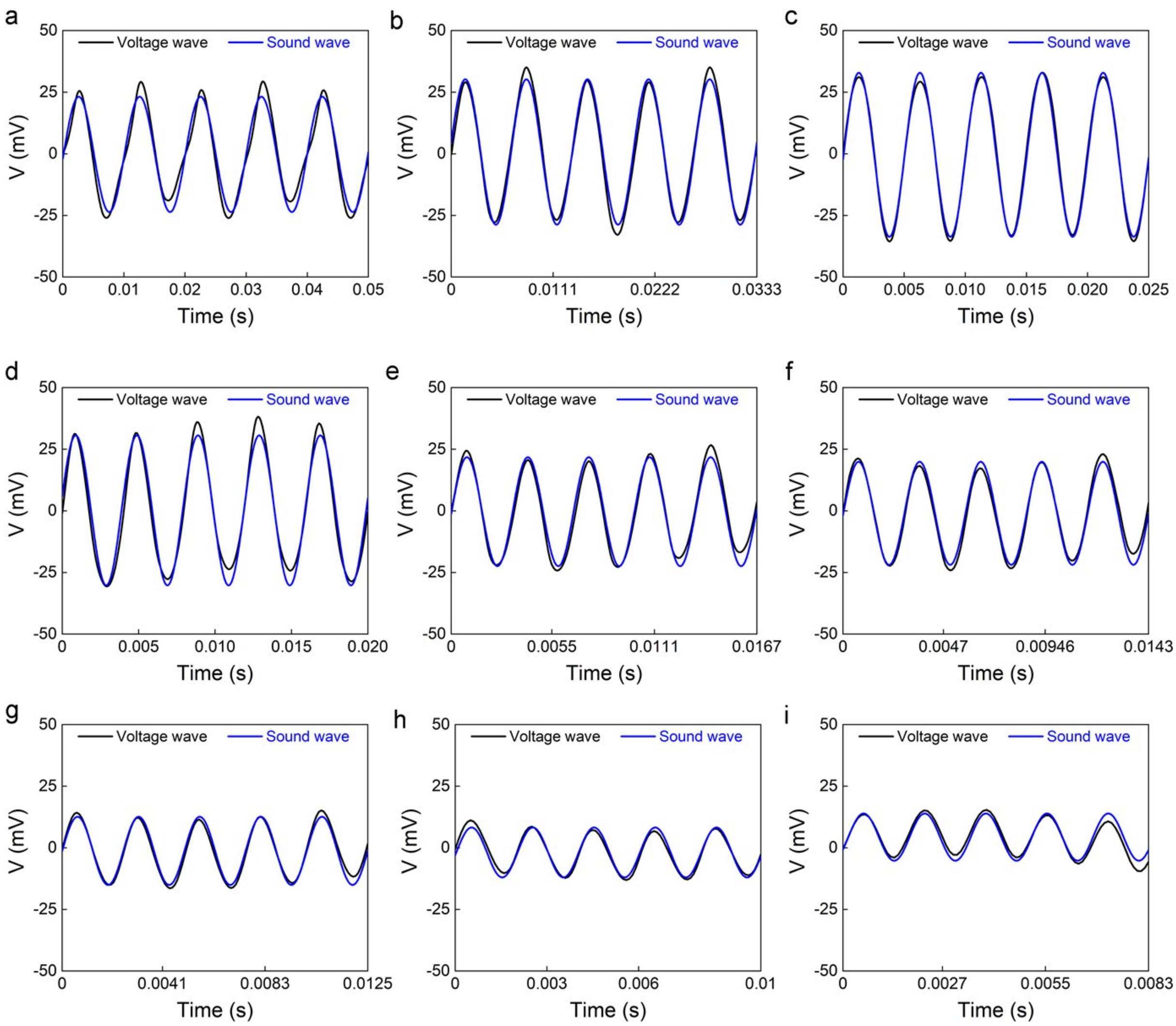

Fig. S12. Fitting of the voltage signals generated by the PAN nanofiber device for the input sound signal at the sound frequencies of (a) 100 Hz, (b) 150 Hz, (c) 200 Hz, (d) 250 Hz, (e) 300 Hz, (f) 350 Hz, (g) 400 Hz, (h) 500 Hz, and (i) 600 Hz. (SPL 75 dB; membrane thickness 30 μm)

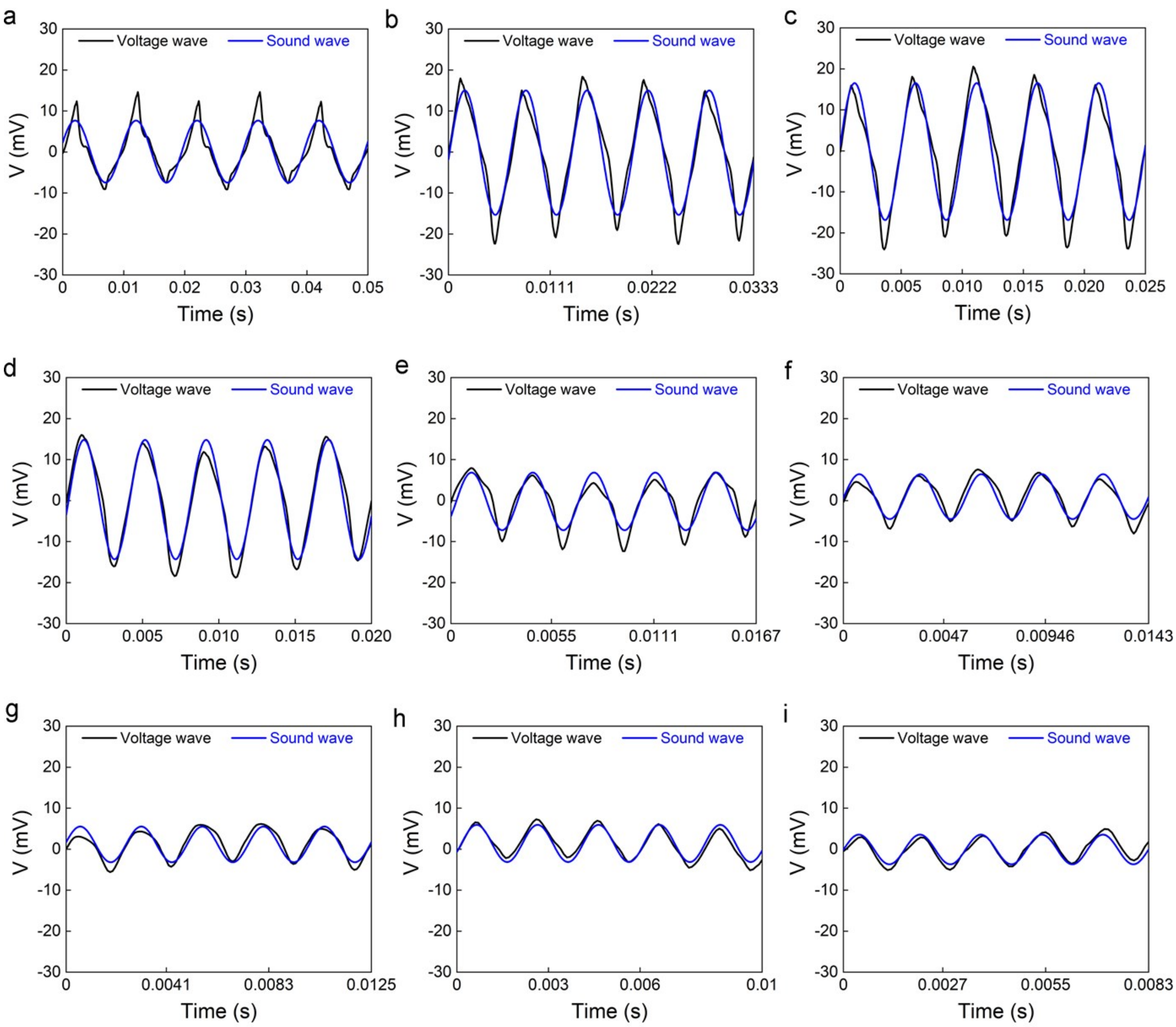

Fig. S13. Fitting of the voltage signals generated by the PVDF nanofiber device for the input sound signal at the sound frequencies of (a) 100 Hz, (b) 150 Hz, (c) 200 Hz, (d) 250 Hz, (e) 300 Hz, (f) 350 Hz, (g) 400 Hz, (h) 500 Hz, and (i) 600 Hz. (SPL 75 dB; membrane thickness 30 μm)

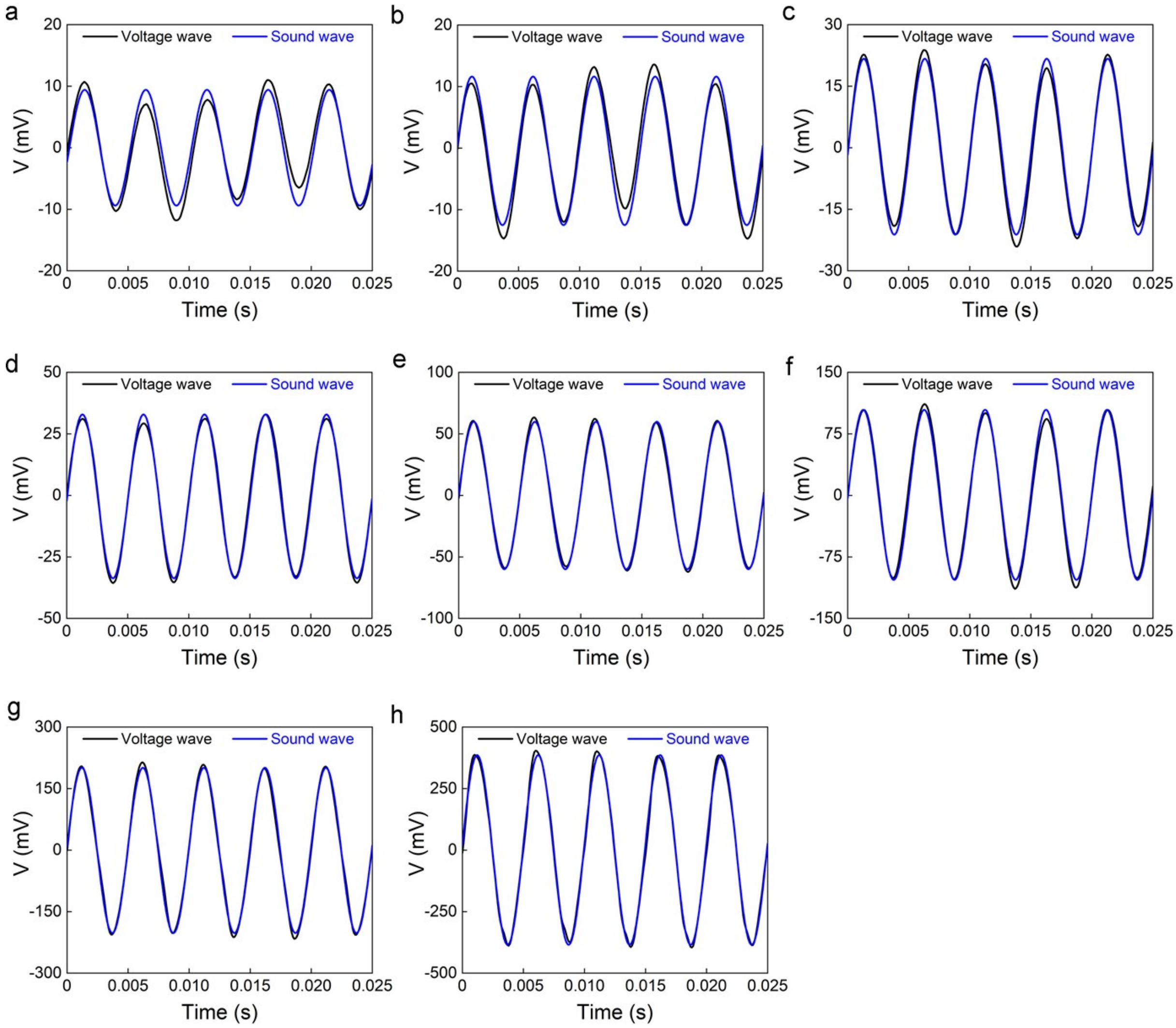

Fig. S14. Fitting of the voltage signals generated by the PAN nanofiber device for the input sound signal at the sound pressure levels of (a) 60 dB, (b) 65 dB, (c) 70 dB, (d) 75 dB, (e) 80 dB, (f) 85 dB, (g) 90 dB, and (h) 95 dB. (Sound frequency 200 Hz, membrane thickness 30 μm)

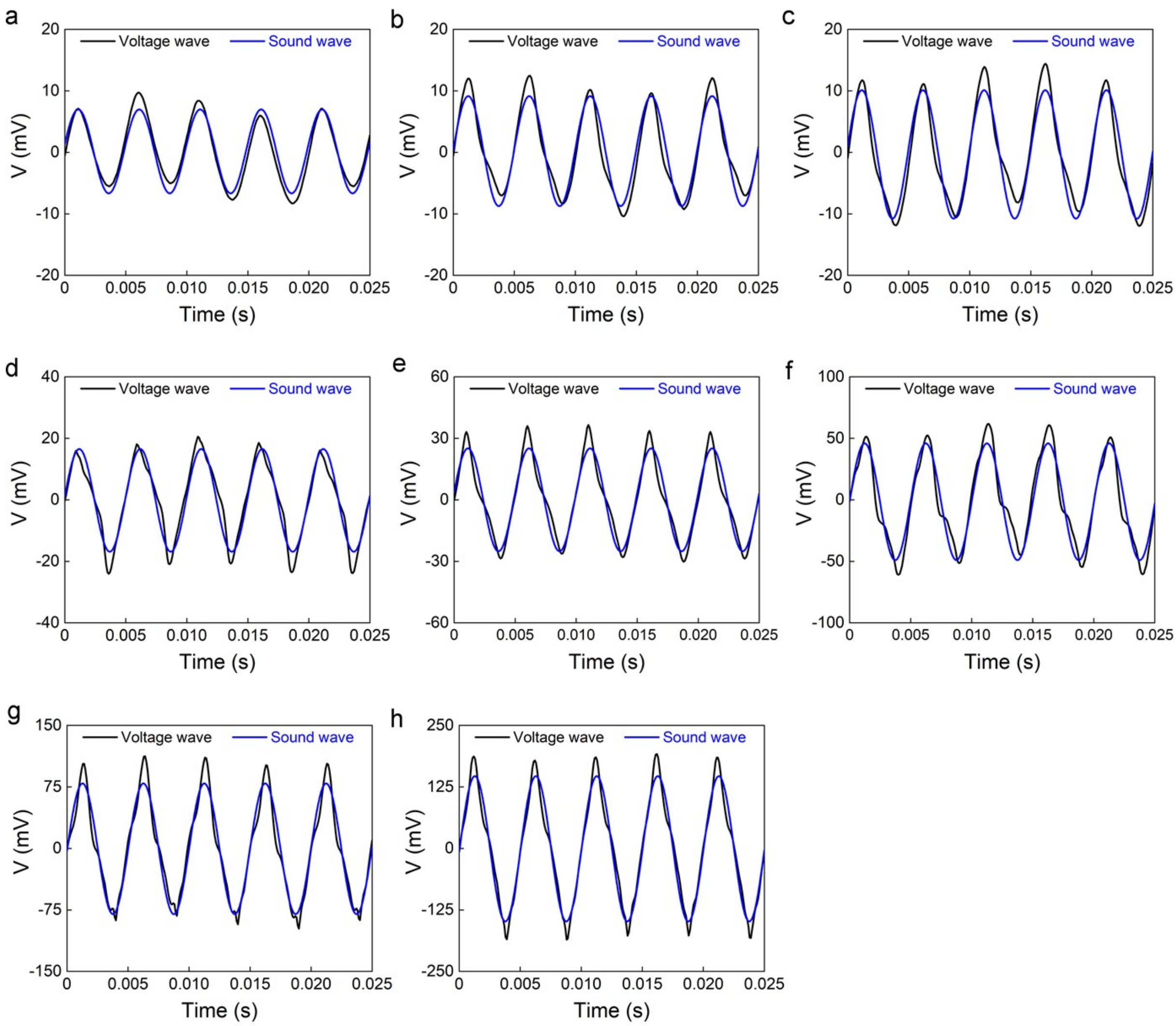

Fig. S15. Fitting of the voltage signals generated by the PVDF nanofiber device for the input sound signal at the sound pressure levels of (a) 60 dB, (b) 65 dB, (c) 70 dB, (d) 75 dB, (e) 80 dB, (f) 85 dB, (g) 90 dB, and (h) 95 dB. (Sound frequency 200 Hz, membrane thickness 30 μm)

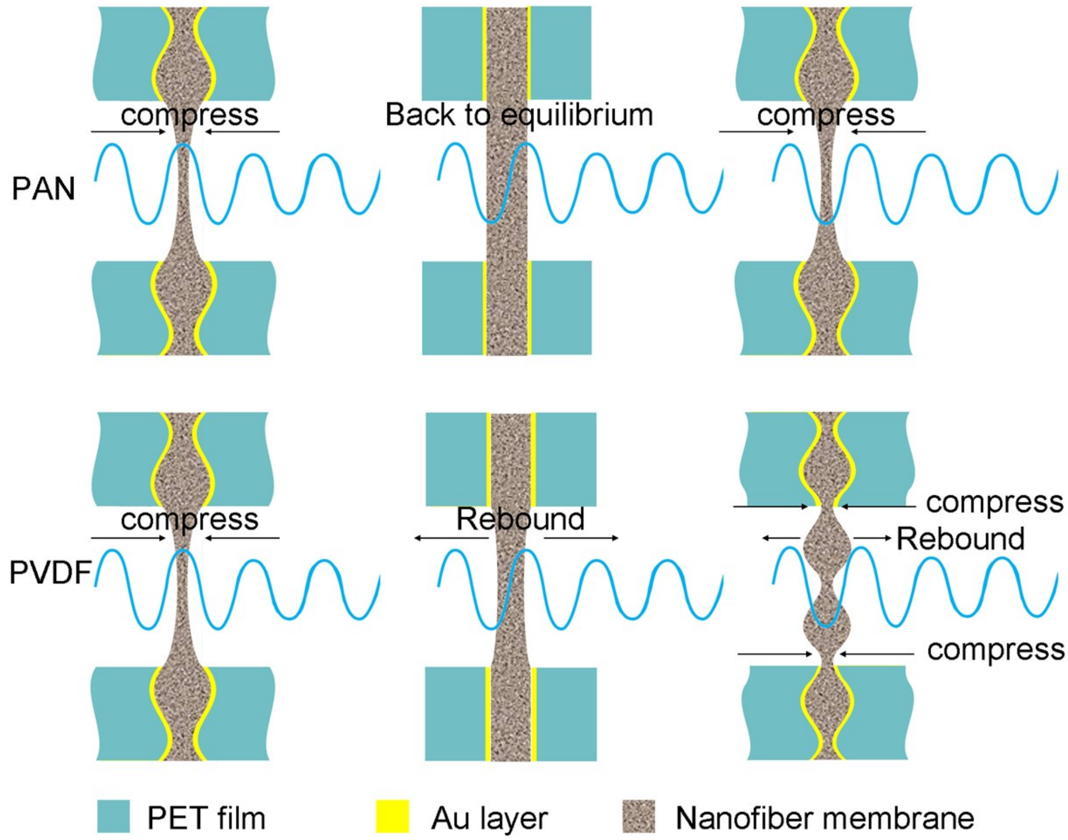

Fig. S16. The proposed nanofiber membrane deformation mechanism under sound.

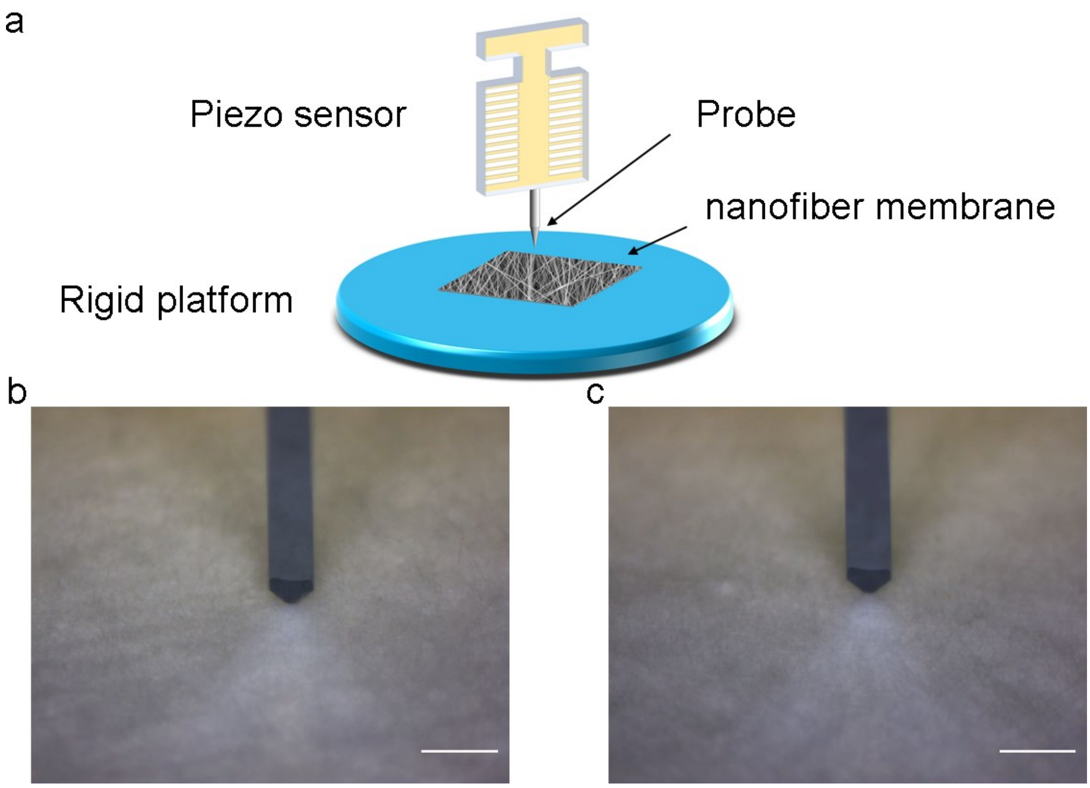

Fig. S17. (a) Schematic illustration of nanomechanical testing apparatus (FemtoTools, FT-MTA03) for the dynamic mechanical analysis (DMA) of the nanofiber membranes; optical microscopic images obtained for (b) PAN nanofiber membrane and (c) PVDF nanofiber membrane (scale bars, 500 μm).

The load presented a sine wave with a periodic frequency of 10 Hz. The load value was set ranging from 50 μN to 200 μN. The nanofiber membrane was subjected to a compressive impact at a certain frequency load, and the hysteresis of its displacement was recorded. The phase angle was obtained.

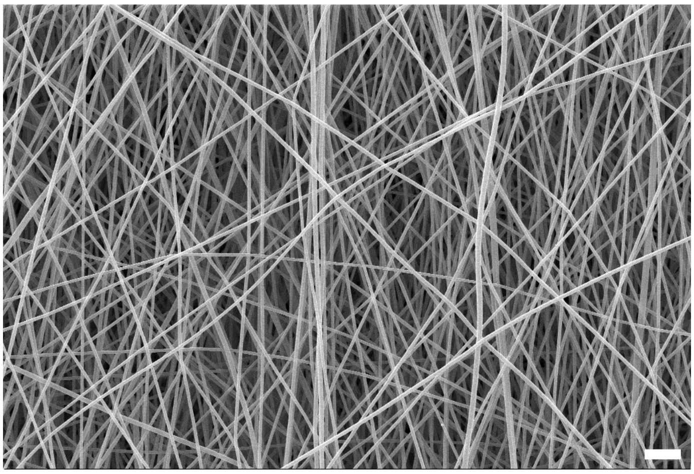

Fig. S18. The SEM image to show the PAN nanofibers after placing in 95 dB sound environment for 2 hours (scale bars, 2 μm).

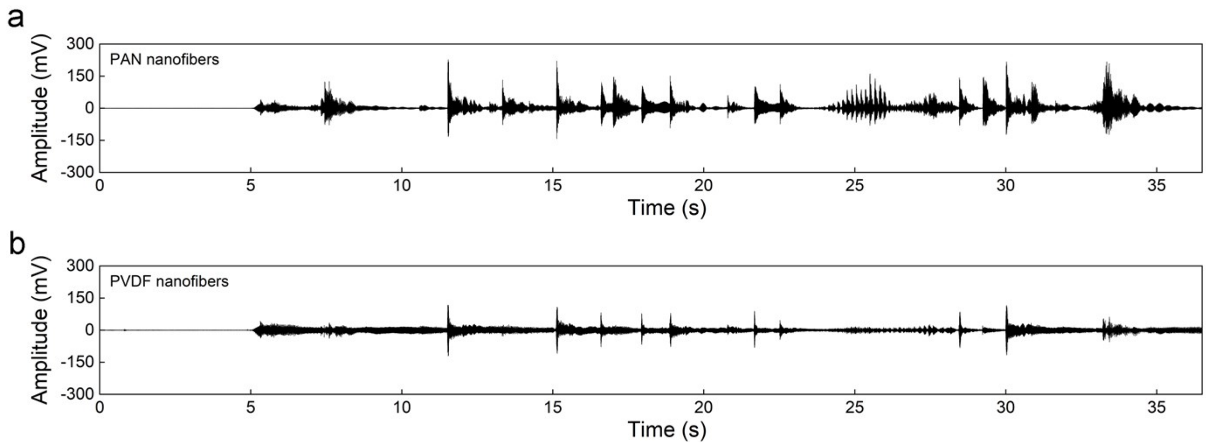

Fig. S19. The voltage signals after FFT band-filter process at 40-60 Hz for (a) PAN nanofiber device, (b) PVDF nanofiber device.

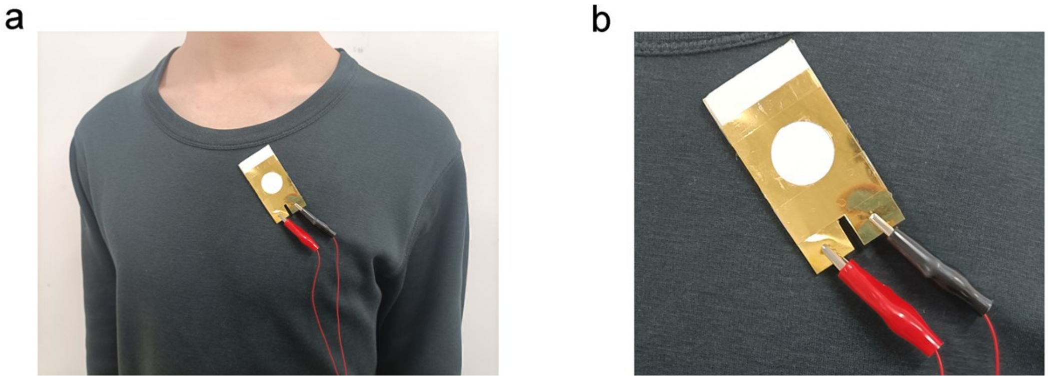

Fig. S20. (a) A digital photo to show the feasibility to be used as a flexible device.

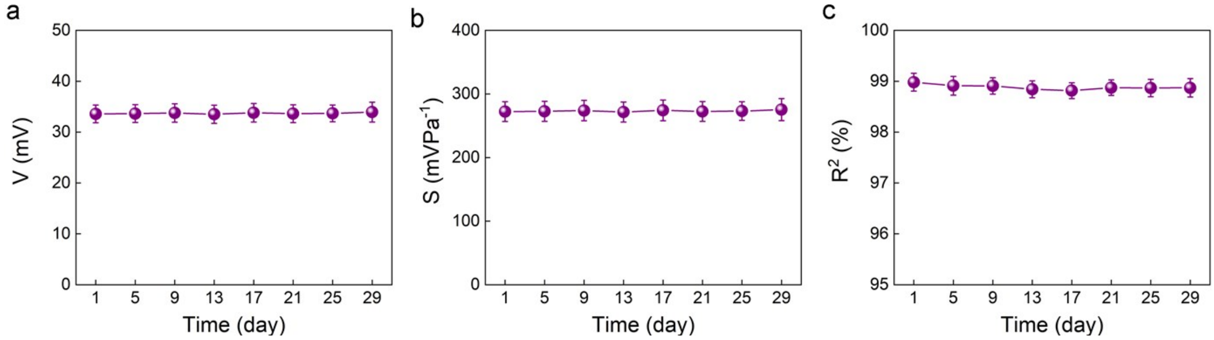

Fig. S21. (A) voltage outputs, (B) sensitivity, and (c) fidelity of the PAN nanofiber device during 29 days of testing. (test condition: 200 Hz 75 dB sound, room temperature and humidity 20% - 30%)

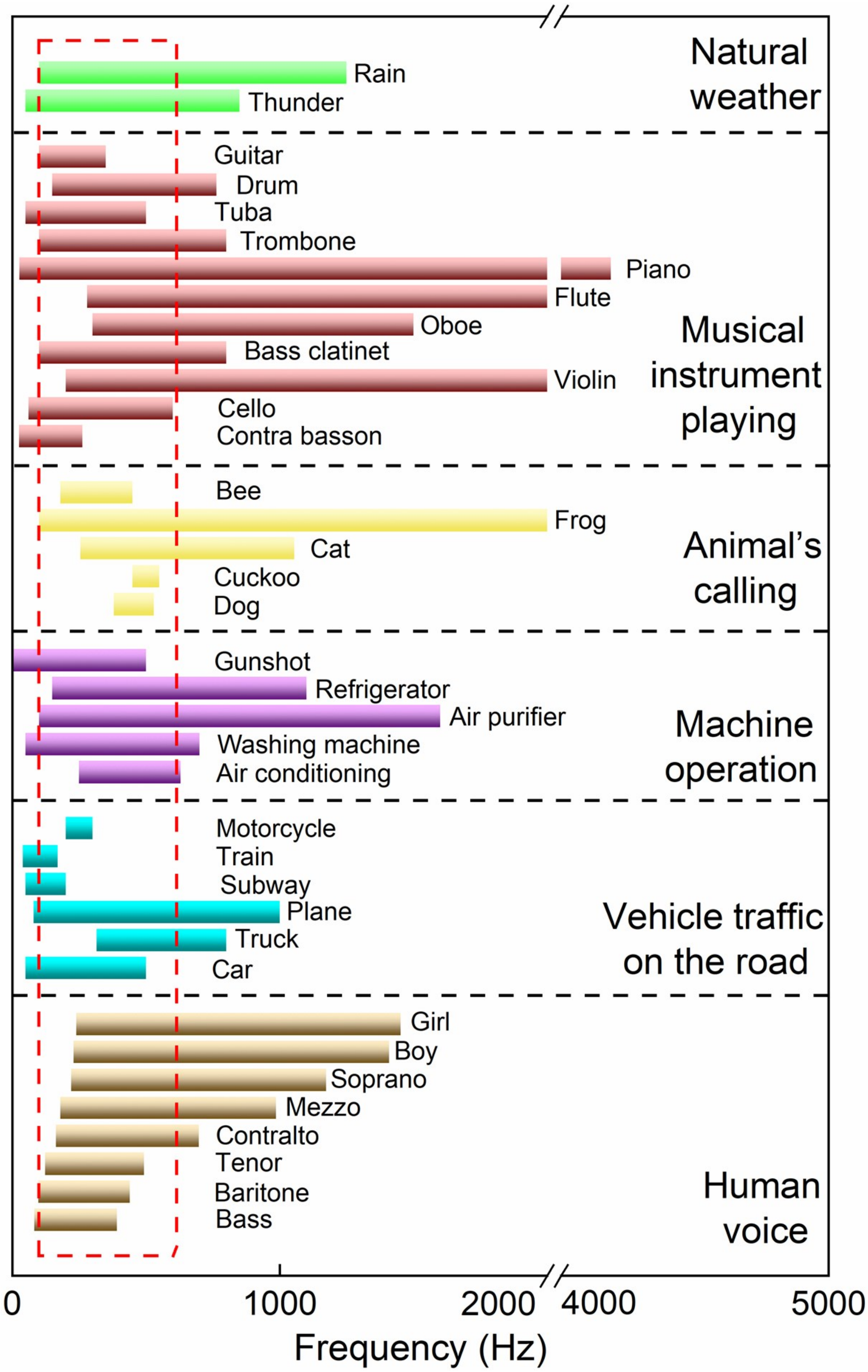

Fig. S22. The sound sources covering the frequency range of 100 Hz-600 Hz in daily life activities [S-1-20].

Table S1. Comparison of different types of acoustoelectric sensors

Method	Principle	External power	Flexibility	Acoustoelectric conversion efficiency	Sensitivity	Signal-to-noise ratio
Electromagnetic	Electromagnetic induction under acoustic vibration	Required	Poor	High	High	High
Triboelectric	Generation of triboelectric charge under acoustic vibration	Self-powered	Good	High	High	High
Piezoelectric	Generation of piezoelectric charge under acoustic vibration	Self-powered	Good	High	High	High

Table S2. A summary of the literature on piezoelectric PVDF for noise harvesting

Materials	Main work	Sound condition	V (V)	I (μA)	P (μW)	Ref.
Electrospun PVDF nanofibers	Flexible all-nonwoven polymer-based piezoelectric generator	220 Hz, 105 dB	5.24	—	4.80	S-21
Electrospun PVDF nanofibers	Flexible sound energy device with the piezoelectric property improved by adding silver nanoparticles.	100 – 400 Hz, 100 dB	0.0592	—	700	S-22
Electrospun PVDF nanofibers	A PVDF nanofiber generator based on different substrates.	100 Hz, 100 dB	0.778	—	—	S-23
Nanoporous PVDF arrays	Preparation of a nanoporous array of PVDF effective generator.	100 Hz, 100 dB	2.6	0.6	—	S-24
PVDF/ZnO composite nanofiber membrane	An acoustoelectric nanogenerator using PVDF/ZnO composite fiber membrane.	140 Hz, 116 dB	1.12	1.6	1.792	S-25
PVDF film	Acoustic harvesting based on PVDF cantilever beams	146 Hz, 110 dB	1.48	—	2.2	S-26
PVDF film	A vibration energy harvesting generator based on a point-defect photonic crystal with PVDF film.	510 Hz	0.0421	—	—	S-27
PVDF film	An energy harvesting based on PVDF cantilever beams and a Helmholtz resonator.	800 Hz	0.22	—	0.1	S-28
PVDF/Graphene composite film	Preparation of a PVDF/graphene film acoustic harvesting device.	280 Hz, 105 dB	7.6	—	—	S-29

Table S3. A summary of the literature on piezoelectric PVDF for sound sensors

Materials	Main work	Sound condition	S	F	SNR (dB)	Ref.
Electrospun PVDF nanofibers	An acoustic sensor based on PVDF nanofiber membrane	220 Hz, 100 dB	266 mV/Pa	—	—	S-30
Electrospun PVDF nanofibers	An acoustic signal sensor that can obtain a wide resource of sound.	100 – 800 Hz	—	High	—	S-31
Electrospun PVDF nanofibers	All-nanofiber-based acoustic sensors that can monitor human motion.	250 Hz, 110 dB	9.2 V/Pa	—	40.9	S-32
PVDF/ZnS composite nanofiber membrane	An acoustoelectric sensor based on PVDF/ZnS composite fiber web.	86 Hz, 100 dB	3 V/Pa	—	—	S-33
PVDF film	An implantable microphone based on flexible PVDF film.	0.1 – 10 kHz, 50 – 60 dB	20 mV/Pa	—	45	S-34

Table S4. A comparison of sound detection properties between PAN and PVDF nanofiber devices

	Sound source		Sound sensing				
	f (Hz)	SPL (dB)	Bandwidth (Hz)	f_{max} (Hz)	S (mV/Pa)	F	L
PAN device		75	100 – 600	1200	-	-	-
		85	100 – 900	1800			
		95	100 – 2000	3000			
PVDF device		75	100 – 320	600	-	-	-
		85	100 – 400	800			
		95	100 – 550	1400			
PAN device	100 – 600	75			45.9 – 273.9	0.939 – 0.993	5.42% – 16.32%
PVDF device					12.2 – 161.5	0.873 – 0.941	14.52% – 29.43%
PAN device	200	60 – 95			271.5 – 351.9	0.938 – 0.995	4.3% – 17.82%
PVDF device					157 – 162.1	0.921 – 0.941	12.94% – 25.93%

Table S5. SNR calculation results for the nanofiber devices and commercial microphone

	$\frac{1}{m}\sum_{i=1}^{m}(V_{p-p})_i$	$2\sqrt[2]{\sum_{j=1}^{n}\frac{{(V_{noise})_i}^2}{n}}$	SNR (dB)
PAN device	34.3	0.6	57.2
PVDF device	22.7	0.6	37.8
Commercial microphone	88.2	1.7	51.9

Table S6. A summary of of acoustoelectric sensors made of different materials

Materials	Method	Sound condition	V (V)	I (μA)	S (mV/Pa)	SNR (dB)	F	Ref.
Ionogels	Resistive	100 Hz (underwater)	—	—	24	50	—	S-35
PTFE nanowires-Cu	Triboelectric	110 Hz, 144.2 dB (underwater)	65	32	—	—	—	S-36
PTFE nanowires-nylon	Triboelectric	A human voice of "*one word*"	—	—	51	—	—	S-37
PTFE film-silver	Triboelectric	200 – 1850 Hz	≈ 0.1 – 0.6	—	—	—	—	S-38
PTFE nanowires-Al	Triboelectric	240 Hz, 70 dB	0.73	0.19	11542.3	—	—	S-39
PTFE nanowires-Cu	Triboelectric	250 Hz, 114 dB	≈ 45	≈ 17	≈ 4489.3	—	—	S-40
FEP film-Au	Triboelectric	100 dB	1.2	—	600	—	—	S-41
PVDF-TrFE nanofibers	Piezoelectric	250 Hz, 90 dB	0.2	—	316.2	—	—	S-42
PVDF-TrFE nanofibers	Piezoelectric	100 – 400 Hz, 78 dB	0.001 – 0.017	—	6.3 – 107	—	—	S-43
PVDF-TrFE film	Piezoelectric	110 dB	≈ 0.4	—	≈ 63.2	—	—	S-11
PZT film	Piezoelectric	250 Hz, 94 dB	0.012	—	12	—	—	S-44
BZT-BCT nanofibers	Piezoelectric	126 Hz, 104 dB	1.0	0.132	315.5	—	—	S-45

Table S7. The main differences between current work and our previous papers [S-30, 46]

Ref.	Materials	Device structure	Main innovation	Sound condition	Key results reported
Nature Communications, 2016, 7, 11108	PVDF	Single hole	First time to report the sound sensing properties of the PVDF nanofiber membrane.	220 Hz, 100 dB	S = 266 mV/Pa
Nano Energy, 2020, 75, 104956	PAN	8 holes	First time to report the application of electrospun PAN nanofiber membrane for harvesting noise.	100 – 500 Hz, 117 dB	V = 58 V I = 12 μA
This work	PAN	Single hole	The first time to report the use of electrospun PAN nanofiber membrane as a sound sensor to detecting middle-intensity sounds. First time to compare the sensing properties between PAN and PVDF nanofiber membranes for application as sound sensors for voice recognition applications.	100 – 600 Hz, 60 – 95 dB	S = 45.9 – 273.9 mV/Pa F = 0.938 – 0.995 SNR = 57.2 dB

f = Frequency, SPL = Sound pressure level, V = Voltage output, I = Current output, P = Power output on an optimized load, f_{max} = Maximum response frequency, S = Sensitivity, F = Fidelity, L = maximum loss ratio, SNR = Signal to noise ratio

Supplementary Videos

Audio S1: the playing effect of the electrical signal recorded by the PAN nanofiber device from a short section of "*high mountains and flowing water*".

Audio S2: the playing effect of the electrical signal recorded by the PVDF nanofiber device from a short section of "*high mountains and flowing water*".

Audio S3: the original signal of "*high mountains and flowing water*".

Audio S4: the playing effect of the electrical signal recorded by the PAN nanofiber device from a short section of "*high mountains and flowing water*" in a high noise environment.

Audio S5: the original signal of "*high mountains and flowing water*" in a high noise environment.

Audio S6: the playing effect of the electrical signal recorded by the PAN nanofiber device from a human voice of "*Hello*".

Audio S7: the original signal of a human voice of "*Hello*".

References

S-1. J. M. Eargle, in *Electroacoustical Reference Data*, Springer US, Boston, MA, 2002, DOI: https://doi.org/10.1007/978-1-4615-2027-6_156, pp. 324-325.
S-2. C. Gough, in *Springer Handbook of Acoustics*, ed. T. D. Rossing, Springer New York, New York, NY, 2014, DOI: https://doi.org/10.1007/978-1-4939-0755-7_15, pp. 567-701.
S-3. D. M. Howard and J. A. S. Angus, in *Acoustics and Psychoacoustics (Fourth Edition)*, eds. D. M. Howard and J. A. S. Angus, Focal Press, Boston, 2010, DOI: https://doi.org/10.1016/B978-0-240-52175-6.00004-1, ch. 4, pp. 167-230.
S-4. E. Murphy and E. A. King, in *Environmental Noise Pollution*, eds. E. Murphy and E. A. King, Elsevier, Boston, 2014, DOI: https://doi.org/10.1016/B978-0-12-411595-8.00005-7, ch. 5, pp. 123-171.
S-5. Y. Nakajima, in *Advanced Tire Mechanics*, Springer Singapore, Singapore, 2019, DOI: https://doi.org/10.1007/978-981-13-5799-2_10, pp. 577-706.
S-6. E. Winer, in *The Audio Expert*, ed. E. Winer, Focal Press, Boston, 2012, DOI: https://doi.org/10.1016/B978-0-240-82100-9.00023-X, ch. 23, pp. 625-652.
S-7. E. G. Berggren, A. M. Kaynia and B. Dehlbom, *Journal of Sound and Vibration*, 2010, **329**, 3999-4016.
S-8. M. J. Buckingham, E. M. Giddens, F. Simonet and T. R. Hahn, *Journal of Computational Acoustics*, 2002, **10**, 445-464.
S-9. V. Cartei, R. Banerjee, A. Garnham, J. Oakhill, L. Roberts, S. Anns, R. Bond and D. Reby, *Hormones and Behavior*, 2020, **117**, 104616.
S-10. G. Degrande, D. Clouteau, R. Othman, M. Arnst, H. Chebli, R. Klein, P. Chatterjee and B. Janssens, *Journal of Sound and Vibration*, 2006, **293**, 645-666.
S-11. Z. Guo, S. Liu, X. Hu, Q. Zhang, F. Shang, S. Song and Y. Xiang, *Sensors and Actuators, A: Physical*, 2020, **306**, 111970.
S-12. J. Y. Jeon, J. You and S. Y. Kim, *The Journal of the Acoustical Society of America*, 2006, **119**, 3412-3412.
S-13. B. Lee, W. Sim, J. Jo and J. Chung, *Journal of Mechanical Science and Technology*, 2020, **34**, 3105-3115.
S-14. S. Lee, S. Heo and C. Cheong, *International Journal of Refrigeration*, 2010, **33**, 1129-1141.
S-15. K. Mazur, S. Wrona and M. Pawelczyk, *Applied Acoustics*, 2019, **146**, 89-95.
S-16. J. A. Parry, K. V. Horoshenkov and D. P. Williams, *Applied Acoustics*, 2020, **164**, 107281.
S-17. J. Xie, M. Towsey, J. L. Zhang and P. Roe, *Artificial Intelligence Review*, 2018, **49**, 375-391.
S-18. X. Yan, S. Lu and J. Li, *Applied Acoustics*, 2016, **106**, 63-76.
S-19. S. C. Yeon, Y. K. Kim, S. J. Park, S. S. Lee, S. Y. Lee, E. H. Suh, K. A. Houpt, H. H. Chang, H. C. Lee, B. G. Yang and H. J. Lee, *Behavioural Processes*, 2011, **87**, 183-189.
S-20. O. Yuhua and Y. Ping, *Journal of Earth System Science*, 2012, **121**, 211-220.
S-21. Y. J. Hwang, S. Choi and H. S. Kim, *Sensors and Actuators, A: Physical*, 2019, **300**, 111672.
S-22. C. M. Wu and M. H. Chou, *Express Polymer Letters*, 2020, **14**, 103-114.
S-23. B. S. Lee, B. Park, H. S. Yang, J. W. Han, C. Choong, J. Bae, K. Lee, W. R. Yu, U. Jeong, U. I. Chung, J. J. Park and O. Kim, *ACS Applied Materials & Interfaces*, 2014, **6**, 3520-3527.
S-24. S. Cha, S. M. Kim, H. Kim, J. Ku, J. I. Sohn, Y. J. Park, B. G. Song, M. H. Jung, E. K. Lee, B. L. Choi, J. J. Park, Z. L. Wang, J. M. Kim and K. Kim, *Nano Letters*, 2011, **11**,

5142-5147.
S-25. B. L. Sun, X. Li, R. Zhao, H. Ji, J. Qiu, N. Zhang, D. Y. He and C. Wang, *Journal of Materials Science*, 2019, **54**, 2754-2762.
S-26. B. Li, A. J. Laviage, J. H. You and Y. J. Kim, *Applied Acoustics*, 2013, **74**, 1271-1278.
S-27. H. Y. Lv, X. Y. Tian, M. Y. Wang and D. C. Li, *Applied Physics Letters*, 2013, **102**, 034103.
S-28. S. Noh, H. Lee and B. Choi, *International Journal of Precision Engineering and Manufacturing*, 2013, **14**, 1629-1635.
S-29. S. Park, Y. Kim, H. Jung, J. Y. Park, N. Lee and Y. Seo, *Scientific Reports*, 2017, **7**, 17290.
S-30. C. Lang, J. Fang, H. Shao, X. Ding and T. Lin, *Nature Communications*, 2016, **7**, 11108.
S-31. N. Shehata, A. H. Hassanin, E. Elnabawy, R. Nair, S. A. Bhat and I. Kandas, *Sensors*, 2020, **20**, 3111.
S-32. M. O. G. Nayeem, S. Lee, H. Jin, N. Matsuhisa, H. Jinno, A. Miyamoto, T. Yokota and T. Someya, *Proceedings of the National Academy of Sciences of the United States of America*, 2020, **117**, 7063-7070.
S-33. A. Sultana, M. M. Alam, S. K. Ghosh, T. R. Middya and D. Mandal, *Energy*, 2019, **166**, 963-971.
S-34. S. Park, X. Y. Guan, Y. Kim, F. X. Creighton, E. Wei, I. Kymissis, H. H. Nakajima and E. S. Olson, *Trends in Hearing*, 2018, **22**, 11.
S-35. M. Wang, L. Yang, J. Adamson, S. Li, Y. Huang, X. Shen, Y. Chen, Q. Zhou and L. Tan, *Acs Applied Electronic Materials*, 2020, **2**, 1295-1303.
S-36. A. F. Yu, M. Song, Y. Zhang, Y. Zhang, L. B. Chen, J. Y. Zhai and Z. L. Wang, *Nano Research*, 2015, **8**, 765-773.
S-37. J. Yang, J. Chen, Y. Su, Q. Jing, Z. Li, F. Yi, X. Wen, Z. Wang and Z. L. Wang, *Advanced Materials*, 2015, **27**, 1316-1326.
S-38. Y. D. Liu, Y. X. Zhu, J. Y. Liu, Y. Zhang, J. Liu and J. Y. Zhai, *Nanoscale Research Letters*, 2018, **13**, 191.
S-39. J. Yang, J. Chen, Y. Liu, W. Q. Yang, Y. J. Su and Z. L. Wang, *ACS Nano*, 2014, **8**, 2649-2657.
S-40. X. Fan, J. Chen, J. Yang, P. Bai, Z. L. Li and Z. L. Wang, *ACS Nano*, 2015, **9**, 4236-4243.
S-41. H. Y. Guo, X. J. Pu, J. Chen, Y. Meng, M. H. Yeh, G. L. Liu, Q. Tang, B. D. Chen, D. Liu, S. Qi, C. S. Wu, C. G. Hu, J. Wang and Z. L. Wang, *Science Robotics*, 2018, **3**, eaat2516.
S-42. W. Wang, P. N. Stipp, K. Ouaras, S. Fathi and Y. Y. S. Huang, *Small*, 2020, **16**, 2070157.
S-43. G. Viola, J. Chang, T. Maltby, F. Steckler, M. Jomaa, J. Sun, J. Edusei, D. Zhang, A. Vilches, S. Gao, X. Liu, S. Saeed, H. Zabalawi, J. Gale and W. Song, *ACS Applied Materials & Interfaces*, 2020, **12**, 34643-34657.
S-44. J. H. Han, J. H. Kwak, D. J. Joe, S. K. Hong, H. S. Wang, J. H. Park, S. Hur and K. J. Lee, *Nano Energy*, 2018, **53**, 198-205.
S-45. N. Y. Cui, X. F. Jia, A. N. Lin, J. M. Liu, S. Bai, L. Zhang, Y. Qin, R. S. Yang, F. Zhou and Y. Q. Li, *Nanoscale Advances*, 2019, **1**, 4909-4914.
S-46. H. Shao, H. Wang, Y. Cao, X. Ding, J. Fang, H. Niu, W. Wang, C. Lang and T. Lin, *Nano Energy*, 2020, **75**, 104956.